

Quantum Efficiency and Crosstalk in Subwavelength HgCdTe Dual Band Infrared Detectors

*Original*

Quantum Efficiency and Crosstalk in Subwavelength HgCdTe Dual Band Infrared Detectors / Vallone, M.; Goano, M.; Tibaldi, A.; Hanna, S.; Wegmann, A.; Eich, D.; Figgemeier, H.; Ghione, G.; Bertazzi, F.. - In: IEEE JOURNAL OF SELECTED TOPICS IN QUANTUM ELECTRONICS. - ISSN 1077-260X. - STAMPA. - 28:2(2022), p. 3800309. [10.1109/JSTQE.2021.3056056]

*Availability:*

This version is available at: 11583/2910088 since: 2021-09-06T08:36:32Z

*Publisher:*

Institute of Electrical and Electronics Engineers Inc.

*Published*

DOI:10.1109/JSTQE.2021.3056056

*Terms of use:*

This article is made available under terms and conditions as specified in the corresponding bibliographic description in the repository

*Publisher copyright*

IEEE postprint/Author's Accepted Manuscript

©2022 IEEE. Personal use of this material is permitted. Permission from IEEE must be obtained for all other uses, in any current or future media, including reprinting/republishing this material for advertising or promotional purposes, creating new collecting works, for resale or lists, or reuse of any copyrighted component of this work in other works.

(Article begins on next page)

# Quantum Efficiency and Crosstalk in Subwavelength HgCdTe Dual Band Infrared Detectors

Marco Vallone, Michele Goano, *Senior Member, IEEE*, Alberto Tibaldi, *Member, IEEE*, Stefan Hanna, Anne Wegmann, Detlef Eich, Heinrich Figgemeier, Giovanni Ghione, *Fellow, IEEE*, and Francesco Bertazzi

**Abstract**—This work investigates the spectral quantum efficiency and inter-pixel crosstalk of a MWIR-LWIR dual band, HgCdTe-based focal plane array (FPA) photodetector (MWIR and LWIR stand for mid- and long-wavelength infrared bands). Pixels are  $10\ \mu\text{m}$ -wide with truncated pyramid geometry and separated by deep trenches. Three-dimensional combined full-wave electromagnetic and electrical simulations in the drift-diffusion approximation allowed to describe the complex, standing-wave-like spectral features resulting from the light interference and diffraction due to the pixels and illuminating beam aperture. The inter-pixel crosstalk for the MWIR operation demonstrated to be very sensible to the trenches depth, in contrast to the LWIR electrooptical response, left almost unchanged. The present work also investigates the causes of performance worsening in the two IR bands when pixel pitch is reduced to  $5\ \mu\text{m}$ , hence well below typical LWIR wavelengths and close to the diffraction limited operation.

**Index Terms**—Infrared detectors, HgCdTe, focal plane arrays, inter-pixel crosstalk, FDTD.

## I. INTRODUCTION

A PUBLICATION by Lawson and co-workers [1] dating 1959 described the outstanding properties of the variable-gap compound  $\text{Hg}_{1-x}\text{Cd}_x\text{Te}$ , which triggered an unprecedented revolution in the development of large-format infrared (IR) Focal Plane Array (FPA) detectors, so at present it is among the most widely used variable-gap semiconductors for IR photodetectors. Among these, “dual-band” are photodetectors capable to operate in two of the standard IR bands, defined as short, mid, long and very long wavelength ( $\lambda$ ) IR bands, respectively SWIR ( $\lambda \in [1, 3]\ \mu\text{m}$ ), MWIR ( $\lambda \in [3, 5]\ \mu\text{m}$ ), LWIR ( $\lambda \in [8, 14]\ \mu\text{m}$ ) and VLWIR ( $\lambda > 14\ \mu\text{m}$ ), and this capability – or, more generally, the multispectral capability – is a central requirement for third-generation, large-format infrared detectors [2], [3], [4], [5], [6], [7], [8], [9], [10], [11], [12], [13], [14].

One of the simplest schemes is known as  $n$ - $p$ - $P$ - $p$ - $n$  triple layer heterostructure: each pixel includes two back-to-back  $p$ - $n$  photodiodes with different cut-off wavelength, separated by a thin, wide bandgap layer (indicated with capital  $P$  in the scheme) acting as barrier, and a single bias contact. The

detector is illuminated from below, and higher-energy photons interact with the shorter-wavelength absorber, which is located closer to the illuminated detector face. Instead, the lower-energy photons are able to reach the longer wavelength section, located above and connected to the bias contact (Fig. 1) [16], [17], [18], [19], [20], [21]. In this class of detectors, known as sequential detectors, either of the  $p$ - $n$  junction can be reverse biased by changing the polarity of the bias voltage, obtaining the spectral response in the corresponding waveband.

The optimization of multispectral IR-FPAs requires considerable design and technology effort, and three-dimensional (3D) simulations of photodetectors with realistic pixel shape can be helpful to save time and reduce cost of fabrication, although they require large numerical resources and careful choice of computational grid [22], [23], [24], [25], [6], [26], [27].

Recent works [28], [29], [30] developed and employed multiphysics approach to reproduce single-color, compositionally graded HgCdTe IR photodetector performance, by means of combined 3D electromagnetic and electrical simulations performed with a commercial simulator by Synopsys [31], which includes an electromagnetic solver (EMW), and an electron transport solver (Sentaurus Device), employed in the drift-diffusion approximation. In those works, simulations of a  $5 \times 5$  miniarray of pixels illuminated by a narrow Gaussian beam focused on its central pixel (CP) provided useful indications about the optimal bias point and effect of pixel geometry on the spectral quantum efficiency (QE) and inter-pixel crosstalk.

The application of the same procedure to dual-band FPAs is not straightforward, especially when heterostructures are concerned, in which carrier density drops to very small values due to reverse bias of semiconductor junctions, unfavoring fast numerical convergence. Hence, a preliminary task was the development and validation of the simulation method against dual-band detector experimental results coming from the literature, as described in detail in Ref. [15].

In the present work, we extend the investigation estimating the impact on QE and inter-pixel crosstalk induced by adopting shallower trenches and reduced pixel pitch size with respect to Ref. [15]. Motivations are twofold: first, in principle trenches should be as deep as possible, in order to prevent carriers photogenerated in a given pixel to diffuse towards neighboring ones, contributing to worsen the captured image definition. However, for technological reasons, getting very deep trenches could be challenging or even not possible.

Second, concerning possible effects, benefits and drawbacks induced by decreasing the pixel size, the scenario is more

M. Vallone, M. Goano, A. Tibaldi, G. Ghione, and F. Bertazzi are with the Dipartimento di Elettronica e Telecomunicazioni, Politecnico di Torino, Corso Duca degli Abruzzi 24, 10129, Torino (TO), Italia e-mail: michele.goano@polito.it

M. Goano, A. Tibaldi, and F. Bertazzi are also with the Istituto di Elettronica e di Ingegneria dell’Informazione e delle Telecomunicazioni, Consiglio Nazionale delle Ricerche c/o Politecnico di Torino.

S. Hanna, A. Wegmann, D. Eich, and H. Figgemeier are with AIM Infrarot-Module GmbH, Theresienstraße 2, D-74072 Heilbronn, Germany

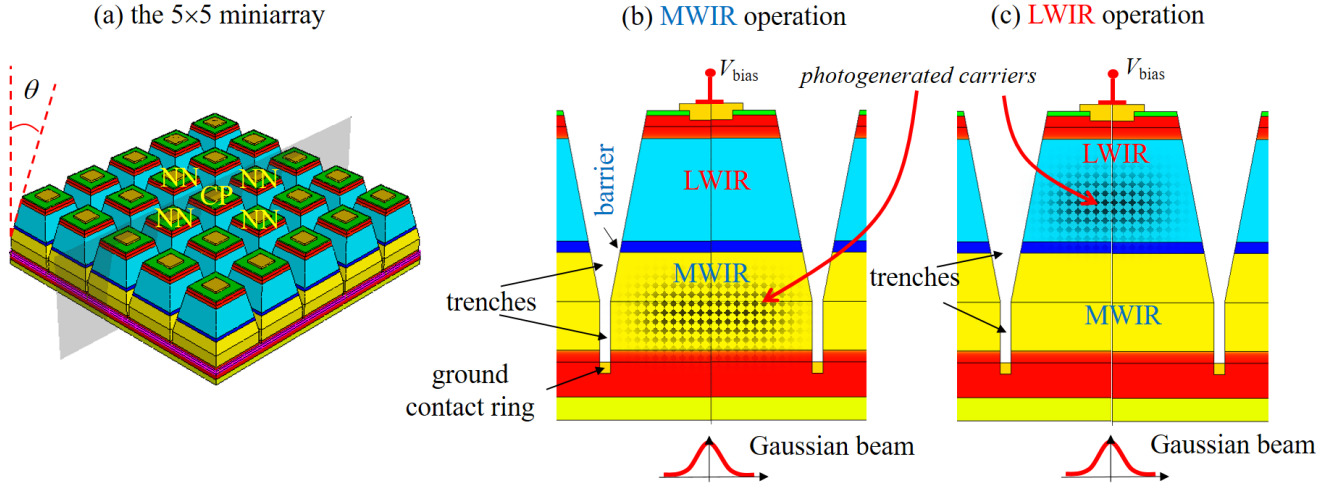


Fig. 1. (a) The 3D miniarray. CP and NN indicate respectively the central (CP) and the nearest neighboring (NN) pixels, and the detector is illuminated from below. In panels (b) and (c) two 2D cutplanes are shown, sketching the operating mode when the light is absorbed respectively by the MWIR and LWIR sections. The angle  $\theta$  has been set to  $12^\circ$ , as in Ref. [15].

complicated. Let us consider a lens-detector system (where a “lens” in realizations may even be a sophisticated camera objective) with focal ratio  $F = f/D$ , where  $D$  and  $f$  are respectively the lens diameter and focal length. In terms of potential image resolution, the optical system performance ranges between two extrema: the *diffraction-limited* case, and the *optics-limited* case [32], [33], [34], [9], [35]. In the first case, the optical frequency is half the sampling frequency (Nyquist criterion), i.e., the pixel pitch  $P_0$  must be

$$P_0 = F\lambda/2, \quad (1)$$

whereas in the second case  $P_0$  is chosen equal to the Airy disk diameter produced by the lens in the focal plane, when imaging a point-like source. The image profile is given by

$$A(r) = 2 \frac{F\lambda}{\pi r} J_1\left(\frac{\pi r}{F\lambda}\right) \quad (2)$$

where  $r$  is the radial coordinate in the focal plane and  $J_1$  is a Bessel function of the first kind of order 1 [36]. Since the first zero of  $J_1(x)/x$  occurs at  $x \approx 3.832$ , i.e.,  $r \approx 3.832F\lambda/\pi = 1.22F\lambda$ , the condition

$$P_0 = 2r \approx 2.44F\lambda \quad (3)$$

identifies an optics-limited system. Considering Eq. (1), a diffraction-limited optical system with  $F = 1$  and  $P_0 = \lambda/2$  should be an optimal choice [32], [9]. In fact, in principle it provides identical performance of a more conventional  $F = 4$  optical system with  $P_0$  four times wider, with the advantage of an overall smaller volume, lower weight and potentially cheaper imaging sensor. As reference values,  $P_0$  ranging in the interval  $[5, 6] \mu\text{m}$  for LWIR and in the interval  $[2, 3] \mu\text{m}$  for MWIR have been recommended [32], [33], [34], [9].

For the present work there is a further complication: we address MWIR-LWIR detectors, therefore the overall wavelength interval extends from  $3 \mu\text{m}$  to  $12 \mu\text{m}$ : it is a hard task to find an optimal choice for  $P_0$ , keeping the same  $F = 1$  “lens” for both IR bands. All the more reason to manage

estimating the impact of different choices for  $P_0$ : therefore, we start considering first the same FPA described in Ref. [15] with  $P_0 = 10 \mu\text{m}$ , then we reduce  $P_0$  to  $7.5 \mu\text{m}$ , and finally down to  $5 \mu\text{m}$ . Most likely there is a price to pay in terms of QE reduction and increased inter-pixel crosstalk, both for smaller pixel size and shallower trenches, therefore a focused study on possible limitations induced by reduced pixel pitch and shallower inter-pixel trenches is desirable.

In section II we describe the detector and the simulation methods, whereas in section III the obtained results are shown, followed by some final considerations in section IV.

## II. SIMULATING A DUAL BAND DETECTOR

Our starting point is the detector described in Ref. [15], modeled as the  $5 \times 5$  MWIR-LWIR pixels miniarray shown in Fig. 1, with pixel pitch  $P_0 = 10 \mu\text{m}$ , illuminated from below by a narrow Gaussian beam centered on the miniarray CP and focused on the  $z = 0$  illuminated face. The need for a  $5 \times 5$  miniarray, instead of the more common choice  $3 \times 3$ , is justified by the increase of calculation accuracy required to describe the inter-pixel crosstalk in presence of interference effects due to internal reflections, more prominent for LWIR operation, since the wavelength is in the order of  $P_0$  [37], [38], [35], [39]. The beam power flux profile at the illuminated face is  $\Phi(r) = \Phi_0 \exp(-2r^2/w_0^2)$ , where  $\Phi_0 = 1 \text{ mW cm}^{-2}$  is the optical power flux along the beam axis,  $r$  is the radial distance from it, and  $w_0$  is the beam waist radius, set to  $2.5 \mu\text{m}$  for all the simulations.

### A. Detector detailed structure

The simulated MWIR-LWIR miniarray consists of a heterostructure with doping scheme  $N^+ - \nu - P^+ - \pi - N^+$  (conventionally, lower case Greek letters refer to low-doped absorber regions, whereas upper case letters refer to layers with a bandgap wider than absorbers). It is composed by a  $1.5 \mu\text{m}$ -thick  $\text{Hg}_{0.59}\text{Cd}_{0.41}\text{Te}$   $N^+$ -SWIR donor doped ( $N_D = 2 \times 10^{17}$

cm<sup>-3</sup>) contact layer grown on a CdTe substrate, followed by two  $\nu$ - and  $\pi$ -absorbers with different bandgap and doping, separated by a  $P^+$ -SWIR barrier, and by a 0.5  $\mu\text{m}$ -thick Hg<sub>0.68</sub>Cd<sub>0.32</sub>Te donor-doped ( $N_D = 2 \times 10^{17} \text{ cm}^{-3}$ ) cap layer. The  $\nu$ - and  $\pi$ -absorbers are respectively a 4.2  $\mu\text{m}$ -thick low donor-doped ( $N_D = 10^{15} \text{ cm}^{-3}$ ) Hg<sub>0.705</sub>Cd<sub>0.295</sub>Te (MWIR) and a 4.4  $\mu\text{m}$ -thick low acceptor-doped ( $N_A = 5 \times 10^{15} \text{ cm}^{-3}$ ) Hg<sub>0.81</sub>Cd<sub>0.19</sub>Te (LWIR) layer, and they are separated by a 0.5  $\mu\text{m}$ -thick acceptor-doped ( $N_A = 5 \times 10^{17} \text{ cm}^{-3}$ ) Hg<sub>0.55</sub>Cd<sub>0.45</sub>Te  $P^+$ -SWIR barrier. To provide a realistic description of the geometry, a 0.5  $\mu\text{m}$ -thick transition layer with linear composition profile is inserted to connect the SWIR contact layer to the MWIR absorber, and another similar one connects the LWIR absorber to the cap layer.

Deep triangular trenches define the pixels, giving them a truncated pyramid shape with 10  $\mu\text{m}$  wide square base. The angle  $\theta$  of the mesa sidewalls is set to 12° with respect to the pixel vertical axis, a value that should assure total reflection at the sidewalls in a large interval of incident radiation wavevector directions [38]. A metal ring surrounds the perimeter of pixels, and it is connected to their SWIR contact layer, providing a common ground for all them. The cap layer of each pixel is connected to a square metallic layer (the bias contact) via an opening in a 0.3  $\mu\text{m}$  thick CdTe passivation layer, which covers the pixel upper face.

## B. Material Parameters

The dependence of HgCdTe electric and optical properties on composition, doping and temperature was taken into account according to the models reported in Ref. [35] (Table I), without including possible doping-induced plasma effects in the complex refractive index, e.g., Burstein-Moss effect and free carrier absorption, [40], [41]. Electrical simulations were obtained considering Auger (modeled as in Ref. [42]) and Shockley-Read-Hall (SRH) as generation-recombination processes, neglecting instead the radiative term. Extensive discussion about this important point can be found in Ref. [43] and references therein. SRH recombination processes were modeled as in Ref. [44] considering a lifetime around 100  $\mu\text{s}$ , neglecting for simplicity trap-assisted tunneling [45], [46], [47], but keeping into account possible contributions to generation-recombination rate coming from band-to-band tunneling (BTBT), described according to the classical expression by Kane [48]

$$R_{\text{BTBT, Kane}} = \frac{np - n_i^2}{(n + n_i)(p + n_i)} A \mathcal{E}^2 \exp\left(\frac{B}{\mathcal{E}}\right) \quad (4)$$

where, for parabolic barriers, the  $A$  and  $B$  coefficients are [49], [50]

$$A = -\frac{q\sqrt{2m_e}}{4\pi^3\hbar^2\sqrt{E_g}}, \quad B = \frac{\pi\sqrt{m_e}E_g^3}{2\sqrt{2}q\hbar}. \quad (5)$$

Here  $\mathcal{E}$ ,  $E_g$ ,  $m_e$ ,  $q$  and  $\hbar$  are respectively the local electric field, energy gap, electron effective mass, electron charge and reduced Planck's constant, whereas  $n_i$  is the intrinsic density, and  $n$  and  $p$  are the electron and hole densities, respectively. Fermi-Dirac statistics and incomplete dopant ionization were

taken into account, with activation energies for HgCdTe alloys estimated according to Ref. [51], [52]. The computational box included air layers located above and below the miniarray (instead of other filling material, for simplicity), and the optical boundary conditions have been set as absorbing along  $z$  (this is obtained with convolutional perfectly matching layers [53]), and periodic along  $x$  and  $y$ , in order to mimic an infinitely extended pixel array.

## C. Simulation Method

The detector was simulated in dark and under monochromatic Gaussian beam illumination as described in section II, setting the lattice temperature to  $T = 230 \text{ K}$ . According to results obtained in Ref. [15], the optimal polarization voltage to select the MWIR and LWIR bands was found to be respectively  $-0.1 \text{ V}$  and  $0.3 \text{ V}$ , values that in the cited reference have been shown to avoid triggering any BTBT contribution to the dark current, taking full advantage of carrier depletion of absorbers, a requirement of central importance for IR photodetectors. A separate electromagnetic simulation followed by an electric simulation was performed for each wavelength point in the interval  $\lambda_n \in [2, 12] \mu\text{m}$  sampled with a step of 0.1  $\mu\text{m}$ , whereas the power flux along the beam axis was set constant to  $1 \text{ mW cm}^{-2}$ . The simulator EMW section solves the Maxwell equations according to the Finite Differences Time Domain (FDTD) method [54], [55], providing  $A_{\text{opt}}$ , i.e., the absorbed photon density distribution in the detector (number of absorbed photons per unit volume and time).  $A_{\text{opt}}$  is obtained as the divergence of the time-averaged Poynting vector  $\langle \vec{S} \rangle$  [56], [37], [57], [58]

$$A_{\text{opt}}(\lambda_n) = -\frac{\vec{\nabla} \cdot \langle \vec{S}(\lambda_n) \rangle}{hc/\lambda_n}, \quad (6)$$

where the material complex refractive index  $n_r + i\kappa$  is included in  $\vec{S}$  as shown e.g. in Refs. [59], [35], Eqs. (8-10). Here  $h$  is the Planck constant, and  $c$  is the light velocity in vacuum. The optical generation rate distribution into the detector due to interband optical absorption is given by  $G_{\text{opt}} = \eta A_{\text{opt}}$  and it enters as a source term in the electron and hole continuity equations, to be self-consistently solved with Poisson equation and Fermi distribution expressions as described in detail e.g. in Ref. [35]. The quantum yield  $\eta$ , defined as the fraction of absorbed photons which are converted to photogenerated electron-hole pairs, was assumed to be unitary.

The presence of layers with compositional grading along the growth direction is a complication for FDTD, which was overcome according to the method outlined in Ref. [28], which allows to treat the complex refractive index as piecewise constant. As a last remark, the staircase discretization should be fine enough to guarantee a small reflection coefficient between adjacent sublayers in the compositionally graded layers (see Ref. [28] for a discussion on this point).

## D. Figures of merit

We do not address in this paper the issues connected to dark current reduction and the study of the generation-recombination mechanisms. Much effort is made by several

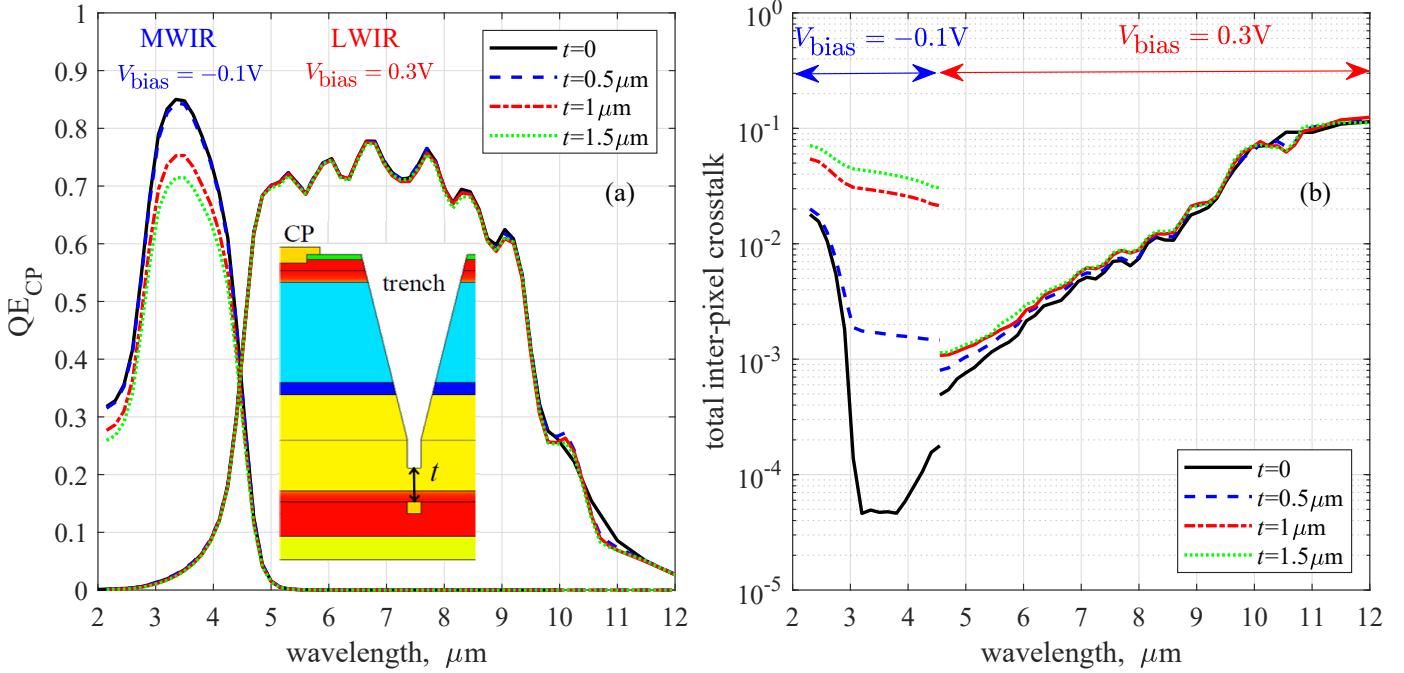


Fig. 2. (a) The external quantum efficiency  $QE_{CP}$ , and (b) the total inter-pixel crosstalk  $C_{NNs}$  for the four considered trench depth variants. In the inset of panel (a) the meaning of the parameter  $t$  is shown.

research groups both from academia and industry towards the minimization of dark current, especially in view of room temperature operation, and a dedicated paper would be required to address the subject [2], [60], [61], [62], [63], [64], [65], [66], [67]. Specifically for the present photodetector, a study of the dark current, the relative importance of BTBT, the choice of SWIR barrier height for minimizing the dark current and finding the optimal bias points has been reported in Ref. [15].

The QE and the inter-pixel crosstalk are two among the main figures of merit which characterize photodetectors. The QE the  $i$ -th pixel (intended as external QE) is defined as

$$QE_i = \frac{I_{ph,i}}{qN_{\text{phot},i}} \quad (7)$$

where  $N_{\text{phot},i}$  is the photon flux through its illuminated face, treated as a simulation parameter, and  $I_{ph,i} = I_i - I_{\text{dark},i}$  is the net contribution to the current  $I_i$  in the  $i$ -th pixel resulting from the optical photogeneration, having subtracted the dark current  $I_{\text{dark},i}$ .

The ratio  $C_i$  between the photocurrent collected by the electrical contacts of the  $i$ -th pixel and of the CP,

$$C_i(\lambda_n) = \frac{I_{ph,i}(\lambda_n)}{I_{ph,CP}(\lambda_n)}, \quad (8)$$

can be regarded as a possible definition of their *total* inter-pixel crosstalk. Considering in particular the nearest neighboring pixels (NNs) beside the CP, the ratio  $C_{NNs}(\lambda_n)$  depends *a)* on carriers photogenerated in the CP diffusing to the neighboring ones (yielding a *diffusive* crosstalk,  $D_{NNs}(\lambda_n)$ ), and *b)* on carriers directly photogenerated in the NNs by the illuminating Gaussian beam tail [35] (*optical* crosstalk). The latter can be defined as the ratio between carriers photogenerated in one of

the NNs (with volume  $V_{NNs}$ ) and those photogenerated in the CP (with volume  $V_{CP}$ )

$$\mathcal{O}_{NNs}(\lambda_n) = \frac{\int_{V_{NNs}} G_{\text{opt}}(x, y, z; \lambda_n) dx dy dz}{\int_{V_{CP}} G_{\text{opt}}(x, y, z; \lambda_n) dx dy dz}, \quad (9)$$

whereas the separation of *diffusive* crosstalk can be obtained following the approach described in our previous work [39] and approximated as

$$D_{NNs} \approx C_{NNs} - \mathcal{O}_{NNs}, \quad (10)$$

having exploited the proportionality between the photocurrent and the integral of  $G_{\text{opt}}$  over the pixel volume appearing in the definition of  $\mathcal{O}_{NNs}$ .

### III. SIMULATION RESULTS: TRENCH DEPTH AND PIXEL PITCH EFFECTS

Scope of the present work is to assess the effect of reducing the trench depth (section III-A) and pixel size (section III-B) on the CP quantum efficiency  $QE_{CP}$ ,  $C_{NNs}(\lambda_n)$  and  $\mathcal{O}_{NNs}(\lambda_n)$ , without discussing limitations imposed by the etching technology, possible defects and leakage caused or favored by trenches [68], and the technological issues which arise to obtain very small pixels [51], [9].

#### A. Effects of inter-pixel trenches

In an ideal FPA, each pixel should be perfectly insulated from its neighbors. In planar structures this cannot be rigorously guaranteed, but a proper design of contacts and passivation layer can provide an electrical quasi-insulation. Despite this, an efficient blocking of the lateral diffusion of photogenerated carriers towards neighboring pixels is a

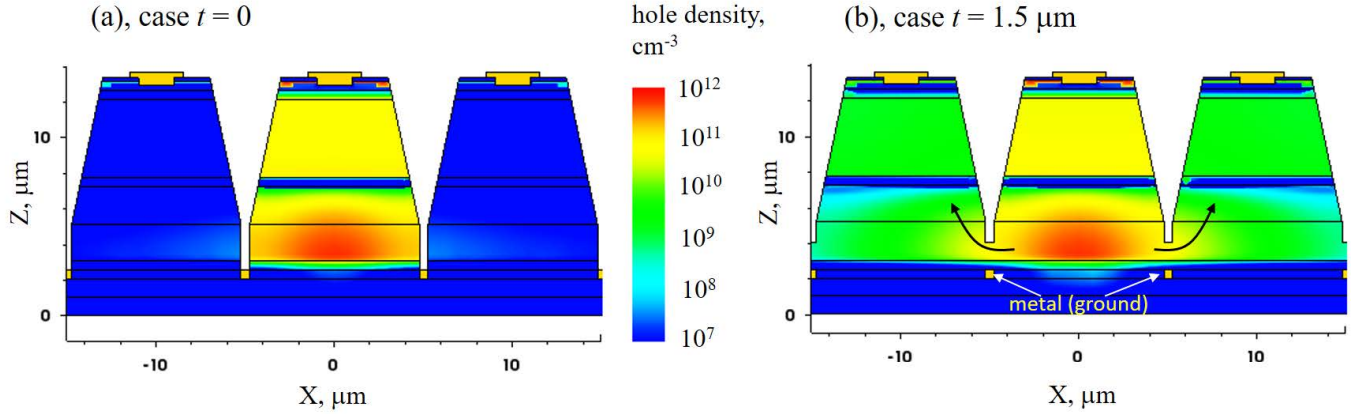


Fig. 3. Effects of trench depth: photogenerated minority carrier density for (a) the reference case ( $t = 0$ ), and (b) for the case  $t = 1.5 \mu\text{m}$ , both for the MWIR operation, shown on the same color scale and obtained in the same calculation conditions:  $V_{\text{bias}} = -0.1\text{V}$ ,  $T = 230\text{K}$ , with a monochromatic  $\lambda = 3.5 \mu\text{m}$  Gaussian beam illumination as described in sec. II.

difficult goal to achieve, although full depleted absorbers can help to this end [29]. This is an important point, since carrier lateral diffusion contribute to blur the images obtained by the photodetector.

An efficient and immediate way to curtail diffusive crosstalk is the adoption of deep trenches between pixels, and in multi-spectral FPAs their adoption is unavoidable [51]. However, the practical difficulty to fabricate trenches which are deep enough to efficiently prevent carrier diffusion towards neighboring pixels can represent a limitation. Aiming at assessing the effect of the trench depth, we considered three variants of the detector simulated in Ref. [15] (hereafter named “reference”), for which the trenches are very deep, as illustrated in Fig. 1. Defining  $t$  as the distance between the trench base and the common ground metal contact, the “reference” has  $t = 0$ . Thus, we considered three alternative possibilities, with  $t = 0.5 \mu\text{m}$ ,  $t = 1 \mu\text{m}$ , and  $t = 1.5 \mu\text{m}$ , and repeated for them all the simulations described in Section II-C, obtaining the results shown in Fig. 2. Concerning the MWIR operation, a progressive increase of  $t$  makes the carriers photogenerated in the CP to diffuse more easily into the NNs, causing a substantial increase of the MWIR inter-pixel crosstalk. Instead, the MWIR spectral  $\text{QE}_{\text{CP}}$  only undergoes a modest reduction. To get deeper insight, Fig. 3 shows the photogenerated minority carrier density (holes) in case of MWIR operation (monochromatic  $\lambda = 3.5 \mu\text{m}$  Gaussian beam illumination as described in sec. II), for the cases  $t = 0$  (the reference case) and  $t = 1.5 \mu\text{m}$ : considerable diffusion between the trench base and the ground contact is apparent only for the case  $t = 1.5 \mu\text{m}$ . Regarding the LWIR operation, no significant changes have been recorded, as it can be expected by considering the quasi-equivalency of the LWIR crosstalk curves reported in Fig. 2. As a final note and with reference to Fig. 2, the case  $t \approx 0.5 \mu\text{m}$  may represent a good compromise, providing values for  $C_{\text{NNs}}$  in the order of  $10^{-3}$  along the whole MWIR band.

### B. Effects of pixel pitch

High-performance FPAs with pixel dimensions approaching the wavelength scale (Nyquist limit) are under intense investigation [32], [33], [34], [9]. The cited works recommend FPAs with pixel size  $P_0$  ranging between  $5 \mu\text{m}$  and  $6 \mu\text{m}$  for LWIR and between  $2 \mu\text{m}$  and  $3 \mu\text{m}$  for MWIR operation. Therefore it is important to assess the effects of the  $P_0$  reduction, starting from the value of  $P_0 = 10 \mu\text{m}$  considered for the “reference” FPA, towards a target value of e.g.  $5 \mu\text{m}$ . Regarding trench depth, we set  $t = 0.5 \mu\text{m}$ , which represents a good starting point and an acceptable trade-off between technological feasibility and expected performance (sec. III-A).

Multiphysics simulations as described in sec. II-C provided the results represented by Fig. 4, where the  $\text{QE}_{\text{CP}}$  and the total inter-pixel crosstalk  $C_{\text{NNs}}$  are shown for  $P_0 = 5, 7.5$  and  $10 \mu\text{m}$ . Spectra show complex, standing-wave-like spectral features, resulting from the internal backreflections and light diffraction due to the pixels and beam aperture. As expected, when  $P_0$  is reduced,  $\text{QE}_{\text{CP}}$  decreases and  $C_{\text{NNs}}$  increases. However, it is noticeable that the effect of  $P_0$  becomes significant only when  $P_0$  is decreased down to  $5 \mu\text{m}$ . In addition, Fig. 5 indicates that for the LWIR band it is  $C_{\text{NNs}} \approx \mathcal{O}_{\text{NNs}}$ : as expected, in the LWIR band the contribution to inter-pixel crosstalk coming from carriers lateral diffusion is negligible, and the whole crosstalk is due to the contribution of  $\mathcal{O}_{\text{NNs}}$ .

An important point to clarify is the behavior of  $\mathcal{O}_{\text{NNs}}$  as function of  $\lambda$ . It is quite apparent that in the LWIR band, apart from oscillations due to light internal back-reflections and the ensuing interference effects,  $\mathcal{O}_{\text{NNs}}$  strongly grows when  $\lambda$  increases. This can be explained considering the expression for the light intensity distribution of a Gaussian beam in the paraxial approximation,

$$I(r, z, \lambda) = I_0 \left( \frac{w_0}{w(z)} \right)^2 \exp(-2r^2/w^2(z, \lambda)), \quad (11)$$

where  $I_0$  is a normalization constant,  $w(z, \lambda) = w_0 \sqrt{1 + (z/z_R(\lambda))^2}$  and  $z_R$  is the Rayleigh distance,

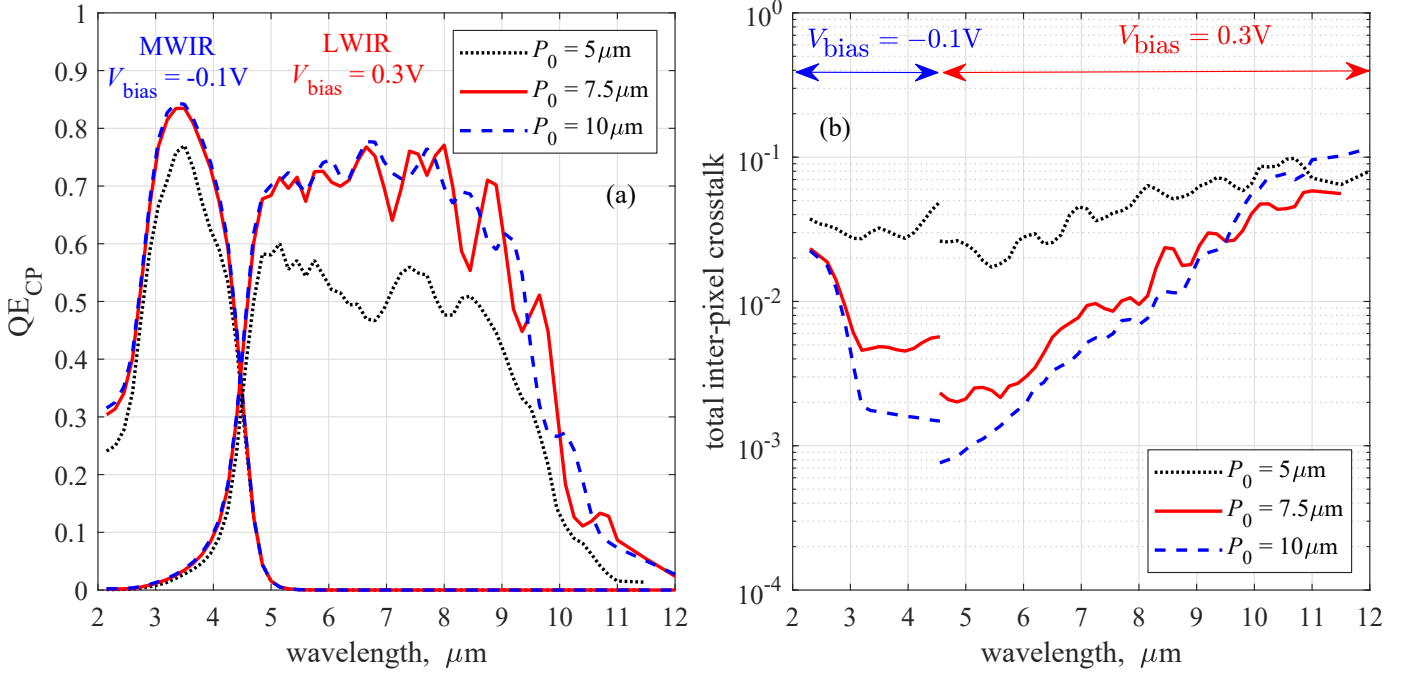


Fig. 4. (a) The external quantum efficiency  $QE_{CP}$ , and (b) the total inter-pixel crosstalk  $C_{NNs}$  for the three considered pixel pitch variants.

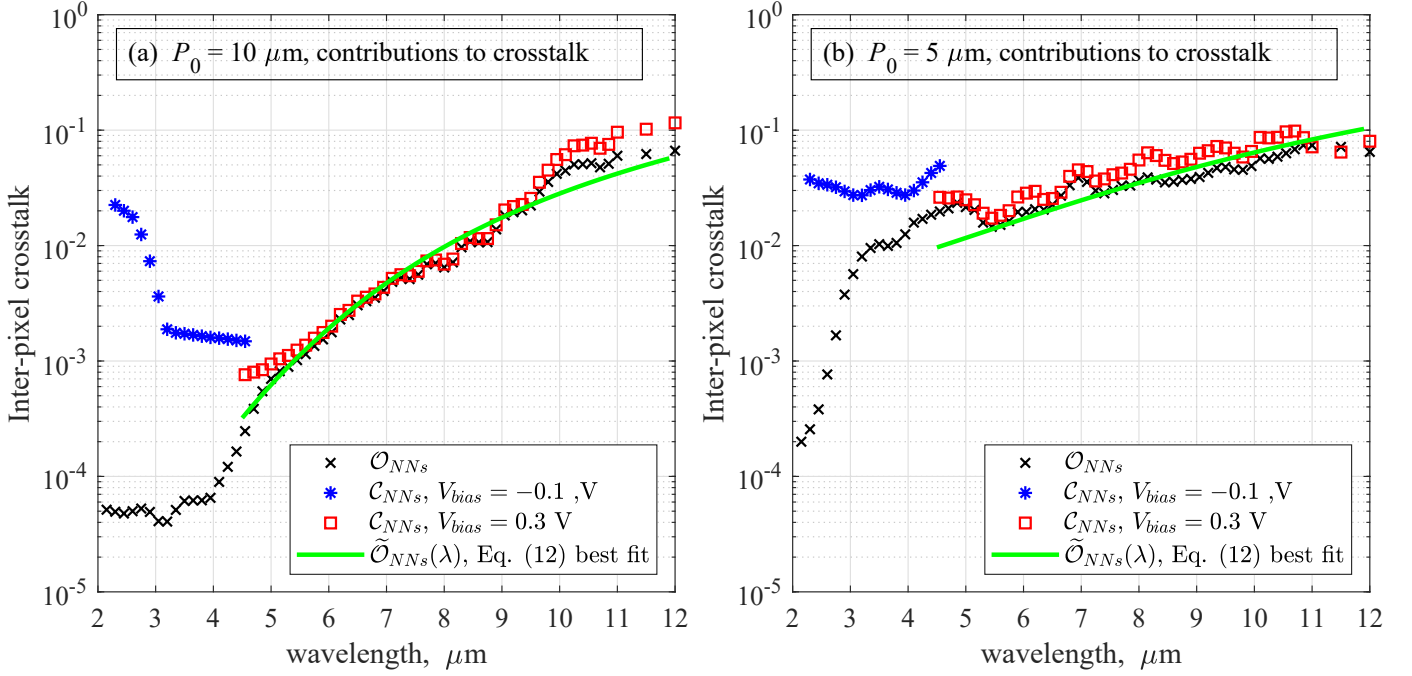


Fig. 5. The optical  $\mathcal{O}_{NNs}$  and total  $C_{NNs}$  inter-pixel crosstalk for the pixel pitch variants  $P_0 = 10 \mu m$  (a) and  $P_0 = 5 \mu m$  (b). The optical crosstalk predicted by Eq. (12) is also shown for comparison (best fit).

given by  $z_R(\lambda) = \pi \omega_0^2 n_r / \lambda$ . Hence the optical inter-pixel crosstalk  $\mathcal{O}_{NNs}(\lambda)$  can be approximated as

$$\tilde{\mathcal{O}}_{NNs}(\lambda) \approx \frac{\int_{P_0/2}^{P_0/2+P_0} I(r, z_0, \lambda)}{\int_0^{P_0/2} I(r, z_0, \lambda)}, \quad (12)$$

where we chose  $z_0 = 5 \mu m$  (just above the pixel pyramid basis), and  $n_r$  is treated just as a fitting parameter (close to the CdTe value in the LWIR band), since the light propagation

takes place in air, in CdTe and HgCdTe layers with different refractive index for different wavelength values, besides the fact that multiple internal reflections occur in the pixels, affecting the effective optical path. In Fig. 5, the result of the nonlinear fitting procedure  $\tilde{\mathcal{O}}$  obtained employing the Eq. (12) is reported, compared to the  $\mathcal{O}_{NNs}(\lambda)$  and  $C_{NNs}(\lambda)$  coming from the numerical simulation. An important outcome is the fact that the inter-pixel crosstalk in the LWIR section

cannot be easily reduced by changing the pixel geometry, since it essentially depends on the beam divergence, hence on the optics which focuses the image. Instead, metalenses, microlenses, and structured interfaces [69] can be viable ways to improve the detector performance, helping in concentrating a beam, which otherwise would considerably diverge beyond its focus plane.

#### IV. CONCLUSIONS

We performed multi-physics simulations of a dual band HgCdTe-based focal plane array with truncated pyramid pixels. The inter-pixel crosstalk due to carrier lateral diffusion resulted very sensible to the trench depth, but only for what concerns the MWIR band, leaving the LWIR band essentially unaffected, at least for the explored cases (see Fig. 2, parameter  $t$ ). Regarding  $QE_{CP}$ , the effects of trench depth resulted quite modest for the MWIR band, and negligible for LWIR.

Concerning the pixel pitch  $P_0$ , we explored the cases  $P_0 = 5, 7.5$  and  $10 \mu\text{m}$ , and a reduction of  $P_0$  was shown to affect both operating bands. However, the effects on  $QE_{CP}$  are quite modest when  $P_0$  is reduced from  $10 \mu\text{m}$  to  $7.5 \mu\text{m}$ , becoming more significant for  $P_0 = 5 \mu\text{m}$ , with a maximum reduction around 30% (Fig. 4). The effects of  $P_0$  on the inter-pixel crosstalk are much more substantial, since  $C_{NNs}$  changes by one order of magnitude in both MWIR and LWIR bands (a little less for the latter, Fig. 5).

Furthermore, the manifest increase of  $C_{NNs}$  for increasing  $\lambda$  in the LWIR band was shown to be totally attributable to  $O_{NNs}$ , in turn coming from the beam divergence, which increases with increasing  $\lambda$  according to Eq. (11) and the expression of  $z_R(\lambda)$ .

#### REFERENCES

- [1] W. D. Lawson, S. Nielsen, E. H. Putley, and A. S. Young, "Preparation and properties of HgTe and mixed crystals of HgTe-CdTe," *J. Phys. Chem. Solids*, vol. 9, no. 3-4, pp. 325-329, 1959.
- [2] M. A. Kinch, "Fundamental physics of infrared detector materials," *J. Electron. Mater.*, vol. 29, no. 6, pp. 809-817, 2000.
- [3] W. E. Tennant, D. Lee, M. Zandian, E. Piquette, and M. Carmody, "MBE HgCdTe technology: A very general solution to IR detection, described by "Rule 07", a very convenient heuristic," *J. Electron. Mater.*, vol. 37, no. 9, pp. 1406-1410, 2008.
- [4] A. Rogalski, J. Antoszewski, and L. Faraone, "Third-generation infrared photodetector arrays," *J. Appl. Phys.*, vol. 105, no. 9, p. 091101, 2009.
- [5] C. A. Keasler and E. Bellotti, "A numerical study of broadband absorbers for visible to infrared detectors," *Appl. Phys. Lett.*, vol. 99, no. 9, p. 091109, 2011.
- [6] J. Schuster, B. Pinkie, S. Tobin, C. Keasler, D. D'Orsogna, and E. Bellotti, "Numerical simulation of third-generation HgCdTe detector pixel arrays," *IEEE J. Select. Topics Quantum Electron.*, vol. 19, no. 5, p. 800415, 2013.
- [7] P. Martyniuk, J. Antoszewski, M. Martyniuk, L. Faraone, and A. Rogalski, "New concepts in infrared photodetector designs," *Appl. Phys. Rev.*, vol. 1, p. 041102, 2014.
- [8] O. Gravrand, J. Rothman, C. Cervera, N. Baier, C. Lobre, J. P. Zanatta, O. Boulade, V. Moreau, and B. Fieque, "HgCdTe detectors for space and science imaging: general issues and latest achievements," *J. Electron. Mater.*, vol. 45, no. 9, pp. 4532-4541, 2016.
- [9] A. Rogalski, P. Martyniuk, and M. Kopytko, "Challenges of small-pixel infrared detectors: a review," *Rep. Prog. Phys.*, vol. 79, no. 4, p. 046501, 2016.
- [10] P. Madejczyk, W. Gawron, P. Martyniuk, A. Koblowski, W. Pusz, J. Pawluczyk, M. Kopytko, J. Rutkowski, A. Rogalski, and J. Piotrowski, "Engineering steps for optimizing high temperature LWIR HgCdTe photodiodes," *Infrared Phys. Technol.*, vol. 81, pp. 276-281, 2017.
- [11] A. Rogalski, P. Martyniuk, and M. Kopytko, "Type-II superlattice photodetectors versus HgCdTe photodiodes," *Progress Quantum Electron.*, p. 100228, 2019.
- [12] R. K. Bhan and V. Dhar, "Recent infrared detector technologies, applications, trends and development of HgCdTe based cooled infrared focal plane arrays and their characterization," *Opto-Electron. Rev.*, vol. 27, no. 2, pp. 174-193, 2019.
- [13] H. Lutz, R. Breiter, D. Eich, H. Figgemeier, and S. Hanna, "Improved high performance MCT MWIR and LWIR modules," in *Infrared Technology and Applications XLV*, vol. 11002, Proceedings of the SPIE, 2019, p. 1100216.
- [14] P. Wang, H. Xia, Q. Li, F. Wang, L. Zhang, T. Li, P. Martyniuk, A. Rogalski, and W. Hu, "Sensing infrared photons at room temperature: from bulk materials to atomic layers," *SMALL*, vol. 15, no. 46, p. 1904396, 2019.
- [15] M. Vallone, M. Goano, A. Tibaldi, S. Hanna, D. Eich, A. Sieck, H. Figgemeier, G. Ghione, and F. Bertazzi, "Challenges in multiphysics modeling of dual-band HgCdTe infrared detectors," *Appl. Opt.*, vol. 59, no. 19, pp. 5656-5663, Jul. 2020.
- [16] J. M. Arias, M. Zandian, G. M. Williams, E. R. Blazejewski, R. E. DeWames, and J. R. Pasko, "HgCdTe dual-band infrared photodiodes grown by molecular beam epitaxy," *J. Appl. Phys.*, vol. 70, no. 8, pp. 4620-4622, 1991.
- [17] P. Ballet, F. Noël, F. Pottier, S. Plissard, J. P. Zanatta, J. Baylet, O. Gravrand, E. D. Borniol, S. Martin, P. Castelein, J. Chamonal, A. Million, and G. Destefanis, "Dual-band infrared detectors made on high-quality HgCdTe epilayers grown by molecular beam epitaxy on CdZnTe or CdTe/Ge substrates," *J. Electron. Mater.*, vol. 33, no. 2, pp. 667-672, 2004.
- [18] R. A. Coussa, A. M. Gallagher, K. Kosai, L. T. Pham, G. K. Pierce, E. P. Smith, G. M. Venzor, T. J. D. Lyon, J. E. Jensen, B. Z. Nosh, J. A. Roth, and J. R. Waterman, "Spectral crosstalk by radiative recombination in sequential-mode, dual mid-wavelength infrared band HgCdTe detectors," *J. Electron. Mater.*, vol. 33, no. 6, pp. 517-525, Jun. 2004.
- [19] A. Rogalski, "HgCdTe infrared detector material: history, status and outlook," *Rep. Prog. Phys.*, vol. 68, pp. 2265-2336, 2005.
- [20] J. Ziegler, D. Eich, M. Mahlein, T. Schallenberg, R. Scheibner, J. Wendler, J. Wenisch, R. Wollrab, V. Daumer, R. Rehm, F. Rutz, and M. Walther, "The development of 3<sup>rd</sup> gen IR detectors at AIM," in *Infrared Technology and Applications XXXVII*, B. F. Andresen, G. F. Fulop, and P. R. Norton, Eds., vol. 8012, Proceedings of the SPIE, Apr. 2011, p. 801237.
- [21] R. K. McEwen, L. Hipwood, S. Bains, D. Owton, and C. Maxey, "Dual waveband infrared detectors using MOVPE grown MCT," in *Detectors and Imaging Devices: Infrared, Focal Plane, Single Photon*, vol. 11002, Proceedings of the SPIE, 2019, p. 1100218.
- [22] D. D'Orsogna, S. P. Tobin, and E. Bellotti, "Numerical analysis of a very long-wavelength HgCdTe pixel array for infrared detection," *J. Electron. Mater.*, vol. 37, no. 9, pp. 1349-1355, 2008.
- [23] J. Schuster and E. Bellotti, "Analysis of optical and electrical crosstalk in small pitch photon trapping HgCdTe pixel arrays," *Appl. Phys. Lett.*, vol. 101, no. 26, p. 261118, 2012.
- [24] E. Bellotti, J. Schuster, B. Pinkie, and F. Bertazzi, "Multi-scale modeling of photon detectors from the infrared to the ultraviolet," in *Infrared Sensors, Devices, and Applications III*, vol. 8868, Proceedings of the SPIE, 2013, p. 88680R.
- [25] B. Pinkie and E. Bellotti, "Large-scale numerical simulation of reduced-pitch HgCdTe infrared detector arrays," in *Infrared Technology and Applications XXXIX*, vol. 8704, Proceedings of the SPIE, 2013, p. 87042S.
- [26] M. Vallone, M. Goano, F. Bertazzi, G. Ghione, R. Wollrab, and J. Ziegler, "Modeling photocurrent spectra of single-color and dual-band HgCdTe photodetectors: Is 3D simulation unavoidable?" *J. Electron. Mater.*, vol. 43, no. 8, pp. 3070-3076, 2014.
- [27] R. DeWames, R. Littleton, K. Witte, A. Wichman, E. Bellotti, and J. Pellegrino, "Electro-optical characteristics of P<sup>+</sup>n <sub>0.53</sub>In<sub>0.47</sub>As hetero-junction photodiodes in large format dense focal plane arrays," *J. Electron. Mater.*, vol. 44, no. 8, pp. 2813-2822, 2015.
- [28] M. Vallone, M. Goano, F. Bertazzi, G. Ghione, S. Hanna, D. Eich, and H. Figgemeier, "FDTD simulation of compositionally graded HgCdTe photodetectors," *Infrared Phys. Technol.*, vol. 97, pp. 203-209, 2019.
- [29] M. Vallone, M. Goano, F. Bertazzi, G. Ghione, A. Palmieri, S. Hanna, D. Eich, and H. Figgemeier, "Reducing inter-pixel crosstalk in HgCdTe detectors," *Opt. Quantum Electron.*, vol. 52, no. 1, p. 25, 2020.
- [30] M. Vallone, M. Goano, F. Bertazzi, G. Ghione, S. Hanna, D. Eich, A. Sieck, and H. Figgemeier, "Constraints and performance tradeoffs



- in Auger-suppressed HgCdTe focal plane arrays," *Appl. Opt.*, vol. 59, no. 17, pp. E1–E8, Jun. 2020.
- [31] *Sentaurus Device User Guide. Version N-2017.09*, Synopsys, Inc., Mountain View, CA, Sep. 2017.
- [32] R. G. Driggers, R. Vollmerhausen, J. P. Reynolds, J. Fanning, and G. C. Holst, "Infrared detector size: how low should you go?" *Opt. Eng.*, vol. 51, no. 6, p. 063202, 2012.
- [33] G. C. Holst and R. G. Driggers, "Small detectors in infrared system design," *Opt. Eng.*, vol. 51, no. 9, p. 096401, 2012.
- [34] W. E. Tennant, D. J. Gulbransen, A. Roll, M. Carmody, D. Edwall, A. Julius, P. Drieske, A. Chen, W. McLevige, S. Freeman, D. Lee, D. E. Cooper, and E. Piquette, "Small-pitch HgCdTe photodetectors," *J. Electron. Mater.*, vol. 43, no. 8, pp. 3041–3046, 2014.
- [35] M. Vallone, M. Goano, F. Bertazzi, G. Ghione, W. Schirmacher, S. Hanna, and H. Figgemeier, "Simulation of small-pitch HgCdTe photodetectors," *J. Electron. Mater.*, vol. 46, no. 9, pp. 5458–5470, 2017.
- [36] M. Abramowitz and I. A. Stegun, Eds., *Handbook of Mathematical Functions with Formulas, Graphs and Mathematical Tables*, ser. National Bureau of Standards Applied Mathematics Series. Washington, D.C.: U.S. Government Printing Office, 1964, no. 55.
- [37] C. Keasler and E. Bellotti, "Three-dimensional electromagnetic and electrical simulation of HgCdTe pixel arrays," *J. Electron. Mater.*, vol. 40, no. 8, pp. 1795–1801, 2011.
- [38] B. Pinkie and E. Bellotti, "Numerical simulation of spatial and spectral crosstalk in two-color MWIR/LWIR HgCdTe infrared detector arrays," *J. Electron. Mater.*, vol. 42, no. 11, pp. 3080–3089, 2013.
- [39] M. Vallone, M. Goano, F. Bertazzi, G. Ghione, S. Hanna, D. Eich, and H. Figgemeier, "Diffusive-probabilistic model for inter-pixel crosstalk in HgCdTe focal plane arrays," *IEEE J. Electron Devices Soc.*, vol. 6, no. 1, pp. 664–673, 2018.
- [40] V. Nathan, "Optical absorption in  $\text{Hg}_{1-x}\text{Cd}_x\text{Te}$ ," *J. Appl. Phys.*, vol. 83, no. 5, pp. 2812–2814, 1998.
- [41] J. Chu and A. Sher, *Physics and Properties of Narrow Gap Semiconductors*. New York: Springer-Verlag, 2008.
- [42] V. C. Lopes, A. J. Syllaios, and M. C. Chen, "Minority carrier lifetime in mercury cadmium telluride," *Semiconductor Sci. Technol.*, vol. 8, no. 6S, pp. 824–841, Jun. 1993.
- [43] M. Kopytko, K. Józwiowski, P. Martyniuk, and A. Rogalski, "Photon recycling effect in small pixel p-i-n HgCdTe long wavelength infrared photodiodes," *Infrared Phys. Technol.*, vol. 97, pp. 38–42, 2019.
- [44] M. Vallone, M. Mandurrino, M. Goano, F. Bertazzi, G. Ghione, W. Schirmacher, S. Hanna, and H. Figgemeier, "Numerical modeling of SRH and tunneling mechanisms in high-operating-temperature MWIR HgCdTe photodetectors," *J. Electron. Mater.*, vol. 44, no. 9, pp. 3056–3063, 2015.
- [45] M. Mandurrino, G. Verzellesi, M. Goano, M. Vallone, F. Bertazzi, G. Ghione, M. Meneghini, G. Meneghesso, and E. Zanoni, "Trap-assisted tunneling in InGaN/GaN LEDs: experiments and physics-based simulation," in *14th International Conference on Numerical Simulation of Optoelectronic Devices (NUSOD 2014)*, Palma de Mallorca, Spain, Sep. 2014, pp. 13–14.
- [46] M. Mandurrino, M. Goano, M. Vallone, F. Bertazzi, G. Ghione, G. Verzellesi, M. Meneghini, G. Meneghesso, and E. Zanoni, "Semiclassical simulation of trap-assisted tunneling in GaN-based light-emitting diodes," *J. Comp. Electron.*, vol. 14, no. 2, pp. 444–455, Jun. 2015.
- [47] M. Mandurrino, G. Verzellesi, M. Goano, M. Vallone, F. Bertazzi, G. Ghione, M. Meneghini, G. Meneghesso, and E. Zanoni, "Physics-based modeling and experimental implications of trap-assisted tunneling in InGaN/GaN light-emitting diodes," *Phys. Status Solidi A*, vol. 212, no. 5, pp. 947–953, 2015.
- [48] E. O. Kane, "Theory of tunneling," *J. Appl. Phys.*, vol. 32, no. 1, pp. 83–89, 1961.
- [49] R. Adar, "Spatial integration of direct band-to-band tunneling currents in general device structures," *IEEE Trans. Electron Devices*, vol. 39, no. 4, pp. 976–981, Apr. 1992.
- [50] K. Józwiowski, M. Kopytko, A. Rogalski, and A. Józwiowska, "Enhanced numerical analysis of current-voltage characteristics of long wavelength infrared n-on-p HgCdTe photodiodes," *J. Appl. Phys.*, vol. 108, no. 7, p. 074519, 2010.
- [51] A. Rogalski, *Infrared Detectors*, 2nd ed. Boca Raton, FL: CRC Press, 2011.
- [52] P. Capper and J. Garland, Eds., *Mercury Cadmium Telluride. Growth, Properties and Applications*. Chichester, U.K.: John Wiley & Sons, 2011.
- [53] J.-P. Berenger, "A perfectly matched layer for the absorption of electromagnetic waves," *J. Comp. Phys.*, vol. 114, no. 2, pp. 185–200, 1994.
- [54] D. Vasileška, S. M. Goodnick, and G. Klimeck, *Computational Electronics. Semiclassical and Quantum Device Modeling and Simulation*. Boca Raton, FL: CRC Press, 2010.
- [55] K. Yee, "Numerical solution of initial boundary value problems involving Maxwell's equations in isotropic media," *IEEE Trans. Antennas Propagation*, vol. 14, no. 3, pp. 302–307, May 1966.
- [56] M. Born and E. Wolf, *Principles of Optics. Electromagnetic Theory of Propagation, Interference and Diffraction of Light*, 7th ed. Cambridge, U.K.: Cambridge University Press, 1999.
- [57] J. Liang, W. Hu, Z. Ye, L. Liao, Z. Li, X. Chen, and W. Lu, "Improved performance of HgCdTe infrared detector focal plane arrays by modulating light field based on photonic crystal structure," *J. Appl. Phys.*, vol. 115, no. 18, p. 184504, 2014.
- [58] O. Akin and H.-V. Demir, "High-efficiency low-crosstalk dielectric metasurfaces of mid-wave infrared focal plane arrays," *Appl. Phys. Lett.*, vol. 110, p. 143106, 2017.
- [59] M. Vallone, M. Goano, F. Bertazzi, G. Ghione, W. Schirmacher, S. Hanna, and H. Figgemeier, "Comparing FDTD and ray tracing models in the numerical simulation of HgCdTe LWIR photodetectors," *J. Electron. Mater.*, vol. 45, no. 9, pp. 4524–4531, 2016.
- [60] S. Maimon and G. W. Wicks, " $nBn$  detector, an infrared detector with reduced dark current and higher operating temperature," *Appl. Phys. Lett.*, vol. 89, no. 15, p. 151109, 2006.
- [61] A. M. Itsuno, J. D. Phillips, and S. Velicu, "Predicted performance improvement of Auger-suppressed HgCdTe photodiodes and p-n heterojunction detectors," *IEEE Trans. Electron Devices*, vol. 58, no. 2, pp. 501–507, Feb. 2011.
- [62] A. M. Itsuno, J. D. Phillips, and S. Velicu, "Mid-wave infrared HgCdTe nBn photodetector," *Appl. Phys. Lett.*, vol. 100, no. 16, p. 161102, Apr. 2012.
- [63] P. Martyniuk and A. Rogalski, "HOT infrared photodetectors," *Opto-Electron. Rev.*, vol. 21, no. 2, pp. 239–257, 2013.
- [64] W. Lei, J. Antoszewski, and L. Faraone, "Progress, challenges, and opportunities for HgCdTe infrared materials and detectors," *Appl. Phys. Rev.*, vol. 2, no. 4, p. 041303, 2015.
- [65] P. Martyniuk, W. Gawron, J. Pawluczyk, A. Keblowski, P. Madejczyk, and A. Rogalski, "Dark current suppression in HOT LWIR HgCdTe heterostructures operating in non-equilibrium mode," *J. Infrared Millim. Waves*, vol. 34, pp. 385–390, 2015.
- [66] J. Schuster, W. E. Tennant, E. Bellotti, and P. S. Wijewarnasuriya, "Analysis of the Auger recombination rate in  $P^+N^-n^-N^-N$  HgCdTe detectors for HOT applications," in *Infrared Technology and Applications XLII*, vol. 9819, Proceedings of the SPIE, 2016, p. 98191F.
- [67] J. Schuster, R. E. DeWames, and P. S. Wijewarnasuriya, "Dark currents in a fully-depleted LWIR HgCdTe P-on-n heterojunction: analytical and numerical simulations," *J. Electron. Mater.*, vol. 46, no. 11, pp. 6295–6305, 2017.
- [68] J. Baylet, O. Gravrand, E. Laffosse, C. Vergnaud, S. Ballerand, B. Avenurier, J. C. Deplanche, P. Ballet, P. Castelein, J. P. Chamonal, A. Million, and G. Destefanis, "Study of the pixel-pitch reduction for HgCdTe infrared dual-band detectors," *J. Electron. Mater.*, vol. 33, no. 6, pp. 690–700, 2004.
- [69] F. Li, J. Deng, J. Zhou, Z. Chu, Y. Yu, X. Dai, H. Guo, L. Chen, S. Guo, M. Lan, and X. Chen, "HgCdTe mid-Infrared photo response enhanced by monolithically integrated meta-lenses," *Sci. Rep.*, vol. 10, no. 1, p. 6372, 2020.



**Marco Vallone** received the M.Sc in Physics from the Università di Torino (Italy) and Ph.D. in Electronic Devices by the Politecnico di Torino (Italy) in 1985 and 2016 respectively. During 1985 - 1999 he was with Telecom Italia, working in a testing and design facility for telecommunications and optoelectronics. In 1999 - 2008 he was with Avago Technologies (a spin-off of Agilent Technologies), working in design and modeling of optoelectronic devices. Since 2008 he holds a Post-Doctoral position at the Politecnico di Torino, where he is currently assistant

professor. His current research activity is focused on the simulation of optoelectronic devices based on narrow- and wide-bandgap semiconductor materials, and on the description of inter- and intra-band quantum scattering processes in the Green's function formalism.



**Michele Goano** (M'98, SM'19) received the Laurea and Ph.D. degrees in electronic engineering from Politecnico di Torino, Turin, Italy, in 1989 and 1993, respectively. In 1994 and 1994, he was a Post-Doctoral Fellow with the Département de Génie Physique, École Polytechnique de Montréal, Montréal, QC, Canada. He joined the faculty of Politecnico di Torino in 1995. He has been a visiting scholar with the School of Electrical and Computer Engineering, Georgia Institute of Technology, Atlanta, GA, USA, with the Department of Information

Technology and Media, Mid-Sweden University, Sundsvall, Sweden, and with the Department of Electrical and Computer Engineering, Boston University, Boston, MA, USA. His current research activity is focused on the simulation of optoelectronic devices based on narrow- and wide-bandgap semiconductor materials.



**Alberto Tibaldi** (M'19) was born in Casale Monferrato, Italy, in 1987. He received the B.Sc., M.Sc., and Ph.D. degrees in electronic engineering from the Polytechnic of Turin, in 2009, 2011 and 2015, respectively. From 2012 to 2019, he was with the Italian National Council of Research (CNR) as a Research Fellow. Since 2019, he has been with the Department of Electronics and Telecommunications, Polytechnic of Turin as an Assistant Professor, where he teaches courses on semiconductor devices and numerical analysis. His scientific interests

mainly regard the multi-physics modeling of optoelectronic devices.

**Stefan Hanna** received the M.Sc. degree in physics and the Ph.D. degree from Universität Bayreuth, Germany, in 2002 and 2008, respectively. He has been with AIM Infrarot-Module GmbH since 2007, working from 2007 to 2010 in the electro-optical characterization of SWIR, LWIR, and VLWIR detectors for space applications within the space projects group of the AIM Division Sensors. From 2008 to 2015, he was a Project Manager of various TRP research and development studies with the European Space Agency, and with the System Design of the AIM Division Space Program from 2014 to 2017, he was working in sensor development within the AIM Division Sensors. Since 2018, he is a Manager with Photodiode Array Development, Division Sensors, AIM.

**Anne Wegmann** received the M.Sc. degree in physics from Universität Münster, Germany, in 2010 and the Ph.D. degree from Universität Heidelberg, Germany, in 2017. She has been with AIM Infrarot-Module GmbH since 2018, working from 2018 to 2019 in the electro-optical characterization of SWIR, LWIR, and VLWIR detectors for space applications within the space projects group of the AIM Division Sensors. From 2018 to 2020 she was a technical manager of a TRP program with the European Space Agency. Since 2020, she has been working in the sensor development group within the AIM Division Sensors.

**Detlef Eich** received the M.Sc. degree in physics and the Ph.D. degree from Universität Würzburg, Germany, in 1996 and 2000, respectively. He has been with AIM Infrarot-Module GmbH, Heilbronn, since 2000. From 2000 to 2009, he was a Development Staff Member with the Development of FPA Technology for CMT IR Photodetectors, Division Sensors, AIM. From 2009 to 2012, he was a Manager with the Development FPA-Technology, Division Sensors. From 2012 to 2014, he was a Manager with Operations Projects, Division Sensors. Since 2014, he has been a Manager with Development, Division Sensors.

**Heinrich Figgemeier** received the M.Sc. degree in physics from Universität Paderborn, Germany, in 1989. From 1989 to 1995, he was with AEG, Heilbronn, as a Development Staff Member with the Development of Liquid Phase Epitaxy for CMT IR Photodetectors. In 1996, he joined AIM Infrarot-Module GmbH, where he is a Manager of Product Planning and FPA-Technology, Division Sensors from 1996 to 2009. From 2009 to 2013, he was a Manager with Division Sensors, AIM, and since 2014, he is the Head of Division Sensors, AIM.



**Giovanni Ghione** graduated cum laude in Electronic Engineering from Politecnico di Torino, Torino Italy in 1981. He is Full Professor in Electronics since 1990. His research activity has been mainly concerned with high-frequency electronics and optoelectronics. He has contributed to the physics-based modelling of compound semiconductor devices, with particular interest in the numerical noise modeling in the small- and large-signal regimes, in the thermal modeling of devices and integrated circuits, and in the modeling of widegap semiconductor devices

and materials. He has also done research in the field of microwave electronics, with contributions in the modeling of passive elements, in particular coplanar components, and in the design of power MMICs. Prof. Ghione was actively engaged since 1985 in research on optoelectronic devices, with application to the modeling and design of near and far-IR photodetectors, electrooptic and electroabsorption modulators, and GAN-based LEDs. Prof. Ghione has authored or co-authored more than 300 research papers on the above subjects and five books. He has been a member of the QPC subcommittee of IEDM in 1997-1998 and in 2006-2007 and Chair in 2008; in 2009-2010 he was the EU Arrangement Co-Chair of IEDM. From 2010 to 2015 he has been chair of the EDS Committee on Compound Semiconductor Devices and Circuits. He has been Chair of the GAAS2003 conference and he has been subcommittee chair in several SCs of the European Microwave Week. Since 2016 he is the Editor in Chief of the IEEE Transactions on Electron Devices. He was President of the Library System of Politecnico from 1997 to 2007. From 2007 to 2015 he was the Head of the Department of Electronics and Telecommunications of Politecnico di Torino.



**Francesco Bertazzi** received the Laurea and Ph.D. degrees in electronics engineering from the Politecnico di Torino, Turin, Italy, in 2000 and 2003, respectively. He was a Visiting Scholar with the Department of Electrical and Computer Engineering at Boston University, Boston, MA. Since 2008 he is professor at the Dipartimento di Elettronica, Politecnico di Torino. His PhD studies were focused on electromagnetic modeling of traveling-wave structures for optoelectronic applications and nonlinear physics-based noise analysis of RF and microwave

devices. His research activities at Boston University included material-theory-based modeling of band structures, vibrational properties, and carrier scattering rates, essential for the study of the complex electronic, transport, and optical properties of novel wide-gap semiconductors, in particular III-nitrides and II-VI oxide semiconductors. His present research activity is focused on density matrix and nonequilibrium Green's function modeling of carrier transport and recombination processes in optoelectronic devices (HgCdTe infrared photodetectors, InGaN light-emitting diodes and VCSELs).